Bimetallic Magnetic Material $[Ni(diamine)_2]_2[Fe(CN)_6]X$ with Two-Dimensional Network Extended by Fe(III)-CN-Ni(II) Linkages

Masaaki Ohba,*,† Hisashi Ōkawa,*,† Nobuo Fukita,† and Yuzo Hashimoto‡

Contribution from the Department of Chemistry, Faculty of Science, Kyushu University, Hakozaki 6-10-1, Fukuoka 812, Japan, and Fukuoka University of Education, 729 Akama, Munakata City, Fukuoka 811-41, Japan

Received June 28, 1996[⊗]

Abstract: Cyanide-bridged bimetallic assemblies $[Ni(pn)_2]_2[Fe(CN)_6]X\cdot cat n H_2O$ (X = ClO_4^- and n = 2 (**1**); X = BF_4^- and n = 2 (**2**); X = PF_6^- and n = 2 (**3**)) and $[Ni(1,1\text{-dmen})_2]_2[Fe(CN)_6]X\cdot n H_2O$ (X = ClO_4^- and n = 2 (**4**); X = BF_4^- and n = 3 (**5**); X = PF_6^- and n = 2 (**6**); X = $CF_3SO_3^-$ and n = 2 (**7**); X = BzO^- and n = 6 (**8**); X = I^- and n = 4 (**9**); X = N_3^- and n = 4 (**10**); X = NCS^- and n = 1 (**11**); X = NO_3^- and n = 4 (**12**)) have been prepared (pn = 1,2-propanediamine, 1,1-dmen = 1,1-dimethylethylenediamine). **7** crystallizes in a monoclinic space group $P2_1/m$ (no. 11), with a = 10.300(6), b = 20.632(4), c = 10.352(7) Å, β = 109.45(4)°, V = 2074(1) Å^3 for Z = 4. **8** crystallizes in a triclinic space group $P\bar{1}$ (no. 2), a = 10.413(6), b = 22.060(6), c = 10.377(3) Å, α = 101.78(2), β = 95.71(4), γ = 77.29(3)°, V = 2272(1) Å^3 for Z = 2. **10** crystallizes in triclinic space group $P\bar{1}$ (no. 2), a = 10.314(1), b = 10.374(1), c = 10.233(1) Å, α = 93.23(1), β = 106.15(1), γ = 86.37(1)°, V = 1045.0(2) Å^3 for Z = 2. In each compounds $[Fe(CN)_6]^{3-}$ coordinates to four $[Ni(1,1\text{-dmen})_2]^{2+}$ cations through four cyano nitrogens on a plane, providing a 2-D sheet of a square structure extended by Fe-CN-Ni linkages. The square with four Fe(III) ions at the corners and four *trans* Ni(II) on the edges shows a slight distortion to a rhombus. A ferromagnetic interaction operates within the sheet in all the compounds. The overall magnetic property is governed by the intersheet separation: a small intersheet separation provides metamagnets (**1**, **2**, **3**, **4**, **6**, **11**) owing to intersheet antiferromagnetic interaction, whereas a large intersheet separation (>10 Å) provides ferromagnets (**5**, **7**, **8**, **9**, **10**, **12**). The ferromagnets became metamagnets on dehydration owing to shortening of the intersheet separation.

Introduction

The design of highly ordered systems of paramagnetic metal centers is a current subject with the aim of providing magnetic materials exhibiting spontaneous magnetization.[1−5] Three pioneering studies appeared at the end of the 1980s: a charge-transfer complex of a columnar structure $[Fe(Me_5Cp)_2]$-[TCNE] (Me_5Cp = pentamethylcyclopentadienyl, TCNE = tetracyanoethylene) (T_C = 4.8 K),[6] a one-dimensional (1-D) oxamato-bridged Mn(II)-Cu(II) complex $\{MnCu(pbaOH)(H_2O)_3\}$ ($pbaOH^{4-}$ = 2-hydroxy-1,3-propylenebis(oxamate) anion) (T_N = 4.6 K),[7] and 1-D radical-bridged complexes $Mn(hfac)_2$(NITR) ($hfac^-$ = hexafluoroacetylacetonate, NITR = 2-R-4,4,5,5-tetramethyl-4,5-dihydro-1-*H*-imidazoyl-1-oxy-3-oxide) (T_N = 7.8 K for R = isopropyl).[8] As evidenced by these studies, the synthetic strategy based on 1-D ferrimagnetic or ferromagnetic chains as the constituents is very promising for molecular-based magnets. However, the interchain interaction is often antiferromagnetic to provide 3-D antiferromagnetic ordering. Thus, recent attention has been directed to the 2-D and 3-D networks of paramagnetic centers.

Cyanide-bridged bimetallic assemblies, derived from $[M(CN)_6]^{n-}$ and simple metal ions, form a family of magnetic materials, and very high T_C or T_N is reported for $CsMn^{II}[Cr^{III}(CN)_6]$ (T_C = 90 K),[9] $CsNi^{II}[Cr^{III}(CN)_6]$ (T_N = 90 K),[10] $Cs_2Mn^{II}[V^{II}(CN)_6]$ (T_N = 125 K),[11] $Cs_{0.75}Cr^{II}_{1.125}[Cr^{III}(CN)_6]$ (T_N = 190 K),[12] and $Cr^{II}_3[Cr^{III}(CN)_6]_2\cdot 10H_2O$ (T_N = 240 K).[12] Those bimetallic assemblies are presumed to have a 3-D structure like Prussian blue extended through M-CN-M′ linkages, but their structures are not well known. Understanding the correlation between the network structure and the magnetism of those bimetallic assemblies is of importance to obtain fundamental bases for high T_C or T_N magnetic materials.

With the hope of gaining insight into the magnetostructural correlation of the cyanide-bridged bimetallic systems, we have initiated a study on bimetallic assemblies comprised of $[M(CN)_6]^{n-}$ and a four-coordinate bis(diamine)nickel(II) $[Ni(diamine)_2]^{2+}$.[13−15] The use of a $[Ni(diamine)_2]^{2+}$ instead

† Kyushu University.
‡ Fukuoka University of Education.
[⊗] Abstract published in *Advance ACS Abstracts,* January 1, 1997.

(1) Kahn, O. In *Molecular Magnetism*; VCH: Weinheim, Germany, 1993.
(2) *Molecular Magnetic Material*; NATO ASI Series E, Gatteschi, D., Kahn, O., Miller, J. S., Palacio, F., Eds.; Kluwer Academic Publishers: Dordrecht, 1990; Vol. 198.
(3) *Proceeding of the Conference on Chemistry & Physics of Molecular-Based Magnetic Materials*. In *Mol. Cryst. Liq. Cryst.* Iwamura, H., Miller, J. S., Eds.; 1993; pp 232−233.
(4) (a) Miller, J. S.; Epstein, A. J. *Angew. Chem., Int. Ed. Engl.* **1994**, *33*, 385. (b) Miller, J. S.; Epstein, A. J. *C&EN* **1995**, October 30.
(5) Tamaki, H.; Zhong, Z. J.; Matsumoto, N.; Kida, S.; Koikawa, M.; Achiwa, N.; Hashimoto, Y.; Ōkawa, H. *J. Am. Chem. Soc.* **1992**, *114*, 6974.
(6) Miller, J. S.; Epstein, A. J.; Reiff, W. M. *Chem. Rev.* **1988**, *88*, 201.
(7) Kahn, O.; Pei, Y.; Verdaguer, M.; Renard, J. P.; Sletten, J. *J. Am. Chem. Soc.* **1988**, *110*, 782.
(8) (a) Caneschi, A.; Gatteschi, D.; Renard, J. P.; Rey, P.; Sessoli, R. *Inorg. Chem.* **1989**, *28*, 1976. (b) Caneschi, A.; Gatteschi, D.; Renard, J. P.; Rey, P.; Sessoli, R. *Inorg. Chem.* **1989**, *28*, 2940. (c) Caneschi, A.; Gatteschi, D.; Renard, J. P.; Rey, P.; Sessoli, R. *Inorg. Chem.* **1989**, *28*, 3314.
(9) Gadet, V.; Mallah, T.; Castro, I.; Verdaguer, M. *J. Am. Chem. Soc.* **1992**, *114*, 9213.
(10) Griebler, W. D.; Babel, D. *Z. Naturforsch.* **1982**, *37b*, 832.
(11) Entley, W. R.; Girolani, G. S. *Science* **1995**, *268*, 397.
(12) Mallah, T.; Thiebaut, S.; Verdaguer, M.; Veillet, P. *Science* **1993**, *262*, 1554.
(13) Ohba, M.; Maruono, N.; Ōkawa, H.; Enoki, T.; Latour, J.-M. *J. Am. Chem. Soc.* **1994**, *116*, 11566.
(14) Ohba, M.; Ōkawa, H.; Ito, T.; Ohto, A. *J. Chem. Soc., Chem. Commun.* **1995**, 1545.

S0002-7863(96)02198-1 CCC: $14.00

of a simple metal ion greatly reduces the complexity in stereochemistry of Prussian Blue analogs because the geometry about the nickel in the resulting bimetallic assemblies is invariably six-coordinate together with two cyano nitrogens. Further, it may be possible to tune the magnetism of the cyanide-bridged bimetallic systems by modifying the $[Ni(diamine)_2]^{2+}$ entity. In our previous study, a bimetallic assembly of the Fe/Ni = 2/3 type, $[Ni^{II}(en)_2]_3[Fe^{III}(CN)_6]_2\cdot 2H_2O$, has been obtained which has a rope-ladder chain structure.[13] In this study, a series of bimetallic assemblies of the Fe/Ni = 1/2 type, $[Ni(diamine)_2]_2[Fe(CN)_6]X\cdot nH_2O$ (diamine = 1,2-propanediamine (pn), 1,1-dimethylethylenediamine (1,1-dmen); X = ClO_4^-, BF_4^-, PF_6^-, $CF_3SO_3^-$, BzO$^-$, I^-, N_3^-, NCS^-, NO_3^-; $n = 2\sim6$), have been synthesized, and their magnetic properties are discussed based on their network and bulk structures. Main emphases are placed on the effects of the diamine, counter anion, and hydration water upon bulk magnetism. A preliminary sudy was reported previously.[14]

Experimental Section

Measurements. Elemental analyses of carbon, hydrogen, and nitrogen were obtained at the Service Center of Elemental Analysis of Kyushu University. Metal analyses were done on a Shimadzu A-A 680 atomic absorption/flame emission spectrophotometer. Infrared spectra were measured on KBr disks with a JASCO IR-810 spectrophotometer. Magnetic susceptibilities were measured by the use of a HOXAN HSM-D SQUID susceptometer in the temperature range of 4.2−100 K (applied magnetic field of 100 G) and by the use of a Faraday balance in the temperature range of 80−300 K (applied magnetic field of 3000 G). Calibrations were made with $Mn(NH_4)_2(SO_4)_2\cdot 6H_2O$ for the SQUID susceptometer and with $[Ni(en)_3]S_2O_3$ for the Faraday balance. Diamagnetic corrections were made with Pascal's constants.[16] Effective magnetic moments were calculated by the equation $\mu_{eff} = 2.828(\chi_M T)^{1/2}$, where χ_M is the molar magnetic susceptibility corrected for diamagnetism of the constituent atoms. The field-cooled magnetization under 3 G, remnant magnetization, and zero-field-cooled magnetization was measured by the SQUID magnetometer. Magnetic hysteresis measurements were made at 4.2 K with a PARC vibrating sample magnetometer in the field range from −20 to +20 kG. Field dependences of magnetization were measured using a flux magnetometer in the applied field up to 75 kG generated by a conventional pulsed technique.

Materials. The Ni(II) complexes $[Ni(diamine)_3]X_2$ (diamine = pn, 1,1-dmen; X = Cl^-, ClO_4^-, PF_6^-) were prepared following the literature method.[17] All chemicals were of reagent grade and used as purchased.

Preparations. $[Ni(pn)_2]_2[Fe(CN)_6]ClO_4\cdot 2H_2O$ (1). $[Ni(pn)_3](ClO_4)_2$ (336 mg, 0.7 mmol) was dissolved in 20 cm^3 of water. To this solution was added an aqueous solution (10 cm^3) of $K_3[Fe(CN)_6]$ (110 mg, 0.33 mmol) at room temperature. The resulting brown mixture was allowed to stand overnight yielding black plates. These were collected by suction filtration, washed with water, and dried *in vacuo* over P_2O_5. Yield: 120 mg (47%). Anal. Calcd for $C_{18}H_{44}N_{14}ClO_6FeNi_2$: C, 28.40; H, 5.83; N, 25.76; Fe, 7.3; Ni, 15.4. Found: C, 28.41; H, 5.79; N, 25.89; Fe, 7.2; Ni, 15.6.

$[Ni(pn)_2]_2[Fe(CN)_6]BF_4\cdot 2H_2O$ (2). This compound was prepared as black plates in a reaction similar to that of **1**, by the use of $[Ni(pn)_3]Cl_2$ instead of $[Ni(pn)_3](ClO_4)_2$ and the addition of $NaBF_4$ (110 mg, 1.0 mmol) to the resulting brown solution. Yield: 100 mg (40%). Anal. Calcd for $C_{18}H_{44}N_{14}BF_4O_2FeNi_2$: C, 28.88; H, 5.92; N, 26.19; Fe, 7.5; Ni, 15.7. Found: C, 28.83; H, 5.96; N, 26.22; Fe, 7.3; Ni, 15.7.

$[Ni(pn)_2]_2[Fe(CN)_6]PF_6\cdot 2H_2O$ (3). This compound was prepared as brown plates in a reaction similar to that of **2**, using $NaPF_6$ instead of $NaBF_4$. Yield: 150 mg (56%). Anal. Calcd for $C_{18}H_{44}N_{14}F_6O_2PFeNi_2$: C, 26.80; H, 5.50; N, 24.30; Fe, 6.9; Ni, 14.5. Found: C, 26.95; H, 5.58; N, 24.38; Fe, 6.7; Ni, 14.3.

$[Ni(1,1\text{-dmen})_2]_2[Fe(CN)_6]ClO_4\cdot 2H_2O$ (4). $[Ni(1,1\text{-dmen})_3](ClO_4)_2$ (365 mg, 0.7 mmol) was dissolved in 20 cm^3 of water. To this solution was added an aqueous solution (10 cm^3) of $K_3[Fe(CN)_6]$ (110 mg, 0.33 mmol) at room temperature, and the resulting brown solution was allowed to stand for 2 days to give black effulorescent crystals. These were collected by suction filtration, washed with water, and dried in the air. Yield: 200 mg (73%). Anal. Calcd for $C_{22}H_{52}N_{14}ClO_6FeNi_2$: C, 32.33; H, 6.41; N, 23.99; Fe, 6.8; Ni, 14.4. Found: C, 32.42; H, 6.40; N, 24.18; Fe, 7.1; Ni, 14.6.

The anhydride $[Ni(1,1\text{-dmen})_2]_2[Fe(CN)_6]ClO_4$ (**4′**) was obtained by heating **4** at 100 °C *in vacuo* for 5 h. Anal. Calcd for $C_{22}H_{48}N_{14}ClO_4FeNi_2$: C, 33.82; H, 6.19; N, 25.10. Found: C, 33.60; H, 6.13; N, 24.96.

$[Ni(1,1\text{-dmen})_2]_2[Fe(CN)_6]BF_4\cdot 3H_2O$ (5). This was prepared as black plates in a reaction similar to that of **4**, by the use of $[Ni(1,1\text{-dmen})_3]Cl_2$ instead of $[Ni(1,1\text{-dmen})_3](ClO_4)_2$ and the addition of $NaBF_4$ (55 mg, 0.5 mmol) to the resulting brown solution. Yield: 150 mg (55%). Anal. Calcd for $C_{22}H_{54}N_{14}BF_4O_3FeNi_2$: C, 32.12; H, 6.62; N, 23.83; Fe, 6.8; Ni, 14.3. Found: C, 32.09; H, 6.55; N, 23.87; Fe, 6.4; Ni, 13.9.

The anhydride $[Ni(1,1\text{-dmen})_2]_2[Fe(CN)_6]BF_4$ (**5′**) was obtained when **5** was heated at 100 °C *in vacuo*. Anal. Calcd for $C_{22}H_{48}N_{14}BF_4FeNi_2$: C, 34.37; H, 6.29; N, 25.51. Found: C, 34.51; H, 6.47; N, 25.36.

Compounds **6**−**12** were prepared in a reaction similar to that for **5** except for using $NaPF_6$ (**6**), $NaCF_3SO_3$ (**7**), sodium benzoate (NaBzO) (**8**), NaI (**9**) NaN_3 (**10**), NaNCS (**11**), or $NaNO_3$ (**12**) instead of $NaBF_4$. They were dehydrated by heating at 100 °C in vacuo to give anhydride or monohydrate compounds **6′**−**11′**.

$[Ni(1,1\text{-dmen})_2]_2[Fe(CN)_6]PF_6\cdot 2H_2O$ (6). Yield: 210 mg (73%). Anal. Calcd for $C_{22}H_{52}N_{14}F_6O_2PFeNi_2$: C, 30.62; H, 6.07; N, 22.72; Fe, 6.5; Ni, 13.6. Found: C, 30.87; H, 6.08; N, 22.82; Fe, 6.2; Ni, 13.3.

The monohydrate $[Ni(1,1\text{-dmen})_2]_2[Fe(CN)_6]PF_6\cdot H_2O$ (**6′**). Anal. Calcd for $C_{22}H_{50}N_{14}F_6OPFeNi_2$: C, 31.27; H, 5.96; N, 23.21. Found: C, 31.54; H, 5.97; N, 23.24.

$[Ni(1,1\text{-dmen})_2]_2[Fe(CN)_6]CF_3SO_3\cdot 2H_2O$ (7). Yield: 150 mg (52%). Anal. Calcd for $C_{23}H_{52}N_{14}F_3O_5SFeNi_2$: C, 31.86; H, 6.05; N, 22.62; Fe, 6.4; Ni, 13.5. Found: C, 31.81; H, 6.02; N, 22.59; Fe, 6.2; Ni, 13.7.

The anhydride $[Ni(1,1\text{-dmen})_2]_2[Fe(CN)_6]CF_3SO_3$ (**7′**). Anal. Calcd for $C_{23}H_{48}N_{14}F_3O_3SFeNi_2$: C, 33.24; H, 5.82; N, 23.60. Found: C, 33.27; H, 5.82; N, 23.53.

$[Ni(1,1\text{-dmen})_2]_2[Fe(CN)_6]BzO\cdot 6H_2O$ (8). Yield: 170 mg (57%). Anal. Calcd for $C_{29}H_{65}N_{14}O_8FeNi_2$: C, 38.23; H, 7.19; N, 21.52; Fe, 6.1; Ni, 12.9. Found: C, 38.19; H, 7.15; N, 21.43; Fe, 5.8; Ni, 12.5.

The monohydrate $[Ni(1,1\text{-dmen})_2]_2[Fe(CN)_6]BzO\cdot H_2O$ (**8′**). Anal. Calcd for $C_{29}H_{55}N_{14}O_3FeNi_2$: C, 42.42; H, 6.75; N, 23.88. Found: C, 42.59; H, 6.64; N, 23.99

$[Ni(1,1\text{-dmen})_2]_2[Fe(CN)_6]I\cdot 4H_2O$ (9). Yield: 220 mg (75%). Anal. Calcd for $C_{22}H_{56}N_{14}IO_4FeNi_2$: C, 30.00; H, 6.41; N, 22.26; Fe, 6.3; Ni, 13.3. Found: C, 30.10; H, 6.41; N, 22.36; Fe, 6.0; Ni, 13.1.

The anhydride $[Ni(1,1\text{-dmen})_2]_2[Fe(CN)_6]I$ (**9′**). Anal. Calcd for $C_{22}H_{48}N_{14}IFeNi_2$: C, 32.67; H, 5.98; N, 24.24. Found: C, 32.54; H, 6.09; N, 24.15.

$[Ni(1,1\text{-dmen})_2]_2[Fe(CN)_6]N_3\cdot 4H_2O$ (10). Yield: 120 mg (45%). Anal. Calcd for $C_{22}H_{56}N_{17}O_4FeNi_2$: C, 33.20; H, 7.09; N, 29.91; Fe, 7.0; Ni, 14.7. Found: C, 33.34; H, 6.96; N, 29.86; Fe, 7.2; Ni, 14.7.

The anhydride $[Ni(1,1\text{-dmen})_2]_2[Fe(CN)_6]N_3$ (**10′**). Anal. Calcd for $C_{22}H_{48}N_{17}FeNi_2$: C, 36.50; H, 6.68; N, 32.89. Found: C, 36.56; H, 6.50; N, 32.89.

$[Ni(1,1\text{-dmen})_2]_2[Fe(CN)_6]NCS\cdot H_2O$ (11). Yield: 100 mg (40%). Anal. Calcd for $C_{23}H_{50}N_{15}OSFeNi_2$: C, 36.44; H, 6.65; N, 27.84; Fe, 7.4; Ni, 15.5. Found: C, 36.21; H, 6.40; N, 22.72; Fe, 6.9; Ni, 15.8.

The anhydride $[Ni(1,1\text{-dmen})_2]_2[Fe(CN)_6]NCS$ (**11′**). Anal. Calcd for $C_{23}H_{48}N_{15}SFeNi_2$: C, 37.33; H, 6.54; N, 28.39. Found: C, 37.04; H, 6.56; N, 28.25.

(15) Ohba, M.; Ōkawa, H.; *Mol. Cryst. Liq. Cryst.* **1996**, *286*, 101.
(16) Boudreaux, E. A.; Mulay, L. N. In *Theory and Applications of Molecular Paramagnetism*; John Wiley & Sons Inc.: New York, 1976; p 491.
(17) Werner, A. *Z. Anorg. Chem.* **1899**, *21*, 210.

Table 1. Crystallographic data for [Ni(1,1-dmen)$_2$]$_2$[Fe(CN)$_6$]CF$_3$SO$_3$·2H$_2$O (**7**), [Ni(1,1-dmen)$_2$]$_2$[Fe(CN)$_6$]BzO·6H$_2$O (**8**), and [Ni(1,1-dmen)$_2$]$_2$Fe(CN)$_6$]N$_3$·4H$_2$O (**10**)

	7	**8**	**10**
formula	$C_{23}F_3H_{52}N_{14}O_5SFeNi_2$	$C_{29}H_{65}N_{14}O_8FeNi_2$	$C_{22}H_{60}N_{17}O_6FeNi_2$
formula weight	867.06	905.12	832.08
crystal system	monoclinic	triclinic	triclinic
space group	$P2_1/m$ (no. 11)	$P\bar{1}$ (no. 2)	$P\bar{1}$ (no. 2)
a	10.300(6)	10.413(6)	10.314(1)
b	20.632(4)	22.060(6)	10.347(1)
c	10.352(7)	10.377(3)	10.223(1)
α	90	101.78(2)	93.23(1)
β	109.45(4)	95.71(4)	106.15(1)
γ	90	77.29(3)	86.37(1)
V	2074(1)	2272(1)	1045.0(2)
Z	2	2	2
D_c	1.388	1.323	1.322
μ (Mo-Kα)	13.55	11.91	12.87
no of reflcns	1682 ($I > 4.0\sigma(I)$)	5791 ($I > 3.0\sigma(I)$)	2498 ($I > 3.0\sigma(I)$)
R^a	0.081	0.058	0.046
$R_w{}^{b,c}$	0.082	0.071	0.060

[a] $R = \sum||F_o| - |F_c||/\sum|F_o|$. [b] $R_w = [(\sum w(|F_o| - |F_c|)^2/\sum F_o^2)]^{1/2}$. [c] $w = 1/\sigma^2(F_o)$.

[Ni(1,1-dmen)$_2$]$_2$[Fe(CN)$_6$]NO$_3$·4H$_2$O (12). Yield: 190 mg (70%). Anal. Calcd for $C_{22}H_{56}N_{15}O_7FeNi_2$: C, 32.38; H, 6.92; N, 25.75; Fe, 6.8; Ni, 14.4. Found: C, 32.55; H, 6.71; N, 25.91; Fe, 6.4; Ni, 14.1.

Heating **12** at 100 °C *in vacuo* gave a partially dehydrated product (**12′**). The extent of dehydration was not determined because the material was highly hygroscopicity.

X-ray Structural Analyses of 7, 8, and 10. Because of the efflorescent nature, single crystals were sealed in a glass capillary and used for structural analyses. Crystallographic data are summarized in Table 1. All the measurements were made on a Rigaku AFC7R diffractometer with graphite monochromated Mo-Kα radiation (λ = 0.71069 Å) and a 12 kW rotating anode generator. The data were collected at 20 ± 1 °C using ω-2θ scan technique to a maximum 2θ value of 50.0° at a scan speed 16.0°/min (in omega). The weak reflections ($I < 10.0\sigma(I)$) were rescanned (maximum of four scans), and the counts were accumulated to ensure good counting statistics. Stationary background counts were recorded on each side of the reflection. The ratio of peak counting time to background counting time was 2:1. The cell parameters were determined by 25 reflections in the 2θ range of 23.19° ≤ 2θ ≤ 26.58° for **7**, 29.41° ≤ 2θ ≤ 30.00° for **8**, and 29.57° ≤ 2θ ≤ 29.88° for **10**. The octant measured was $+h,+k,\pm l$ for **7** and $+h,\pm k,\pm l$ for **8** and **10**. The intensities of the representative reflections were measured after every 150 reflections. Over the course of data collection, the standards for **7** and **10** decreased by 5.1 and 4.9%, respectively, while the standards of **8** increased by 8.0%. A linear correction factor was applied to the data to account for the phenomena. Intensity data were corrected for Lorentz and polarization effects.

The structures were solved using the direct methods and refined using the Fourier techniques. The non-hydrogen atoms were refined anisotropically. Hydrogen atoms were included but not refined. The final positional parameters of non-hydrogen atoms of **7**, **8**, and **10** with their estimated standard deviations are listed in Tables S25, 26, and 27, respectively.

Neutral atom scattering factors were taken from Cromer and Waber.[18] Anomalous dispersion effects were included in F_{calc}; the values for $\Delta f'$ and $\Delta f''$ were those of Creagh and McAuley.[19] The values for the mass attenuation coefficients were those of Creagh and Hubbel.[20] All calculations were performed using the teXsan crystallographic software package of Molecular Structure Corporation.[21]

Results and Discussion

Syntheses and General Properties. In our previous study[14,15] tris(ethylenediamine)nickel(II) $[Ni(en)_3]^{2+}$ was used to prepare crystalline $[Ni(en)_2]_3[Fe(CN)_6]_2\cdot 2H_2O$. In this synthesis, a partial dissociation of $[Ni(en)_3]^{2+}$ into $[Ni(en)_2]^{2+}$ in aqueous solution allowed a slow crystallization of the assembly. This method was adopted in this study for preparing [Ni(pn)$_2$]$_2$[Fe(CN)$_6$]X·*n*H$_2$O (X = ClO_4^- and *n* = 2 (**1**); X = BF_4^- and *n* = 2 (**2**); X = PF_6^- and *n* = 2 (**3**)) and [Ni(1,1-dmen)$_2$]$_2$[Fe(CN)$_6$]X·*n*H$_2$O (X = ClO_4^- and *n* = 2 (**4**); X = BF_4^- and *n* = 3 (**5**); X = PF_6^- and *n* = 2 (**6**); X = $CF_3SO_3^-$ and *n* = 2 (**7**); X = BzO^- and *n* = 6 (**8**); X = I^- and *n* = 4 (**9**); X = N_3^- and *n* = 4 (**10**); X = NCS^- and *n* = 1 (**11**); X = NO_3^- and *n* = 4 (**12**)). Bimetallic assemblies with $[Ni(pn)_2]^{2+}$ were limited to the counter anions ClO_4^-, BF_4^-, and PF_6^-. On the other hand, bimetallic assemblies with $[Ni(1,1\text{-dmen})_2]^{2+}$ were obtained for various counter anions. We have also obtained the corresponding ethylenediamine (en) compounds [Ni(en)$_2$]$_2$[Fe(CN)$_6$]X (X = ClO_4^-, BF_4^-, and PF_6^-) as anhydrides, but they are not included in this study because preliminary results have suggested that the en compounds have a network structure differing from that of **1**−**12** (2-D network as discussed below).

Each bimetallic assembly shows two $\nu_{(C\equiv N)}$ modes near 2140 and 2110 cm^{-1}. The IR band near 2110 cm^{-1} is compared to the $\nu_{(C\equiv N)}$ band of $K_3[Fe(CN)_6]$ (2110 cm^{-1}) and can be attributed to the nonbridging cyanide group. The $\nu_{(C\equiv N)}$ mode near 2140 cm^{-1} is attributed to the bridging cyanide group. The en compounds $[Ni^{II}(en)_2]_2[Fe^{III}(CN)_6]X$ show three $\nu_{(C\equiv N)}$ vibrations at 2140, 2130, and 2110 cm^{-1}, suggesting a network of low symmetry.[13]

Crystal Structures. The structure of **1** was previously determined by X-ray crystallography to have a 2-D network of a square structure.[14] Similar 2-D network structures have been proved for **7**, **8**, and **10** in this study.

Compound 7. Figure 1 shows an ORTEP drawing of the Ni_2Fe trinuclear unit of **7** (the asymmetric unit corresponds to one half of the trinuclear unit). The selected bond distances and angles with their estimated standard deviations are listed in Table 2. The Fe ion is located at the inversion center (0, 0, 0) and the $[Fe(CN)_6]^{3-}$ ion coordinates to four adjacent Ni ions with its four cyano nitrogens (N1, N2, N1*, and N2*) in a plane to form a 2-D square structure (Figure 2a). The Fe−C1−N1−Ni1−N1*−C1*− and Fe−C2−N2−Ni2−N2*−C2*− linkages are running along the *a* and *b* axes, respectively. The intrasheet Fe—Ni1, Fe—Ni2, and Ni1—Ni2 separations are 5.150(3), 5.164(2), and 7.118(3) Å, respectively. The Fe−C−N bond is almost linear, whereas the C−N−Ni bond is slightly bent: the C1−N1−Ni1 and C2−N2−Ni2 angles are 170(1) and 174(1)°, respectively. The square formed by four Fe ions is nearly equilateral (10.300(6) and 10.316(4) Å). The geometries about Ni1 and Ni2 are best depicted as a pseudo octahedron with an Ni−N bond distance of *ca.* 2.10 Å. The Ni2 ion is located on a mirror plane (0.0222, 0.25, −0.0048). The atoms N6, N7, N8, N9, C9, C11, and C12 are also located on the mirror plane. The trifluoromethanesulfonate anion resides within the square and S1, O2, C14, and F2 atoms are also located on the mirror plane. The atoms C9, C12, and C13 have large thermal factors, which is the result of poor reflection data due to the efflorescent nature of the crystal.

(18) Cromer, D. T.; Waber, J. T. In *International Tables for X-ray Crystallography, Vol. IV*; The Kynoch Press: Birmingham, England, 1974.

(19) Creagh, D. C.; McAuley, W. J. In *International Tables for Crystallography, Vol. C*; Kluwer Academic Publishers: Boston, 1992.

(20) Creagh, D. C.; Hubbell, J. H. In *International Tables for Crystallography, Vol. C*; Kluwer Academic Publishers: Boston, 1992.

(21) teXsan: Crystal Structure Analysis packege, Molecular Structure Corporation: 1985; 1992.

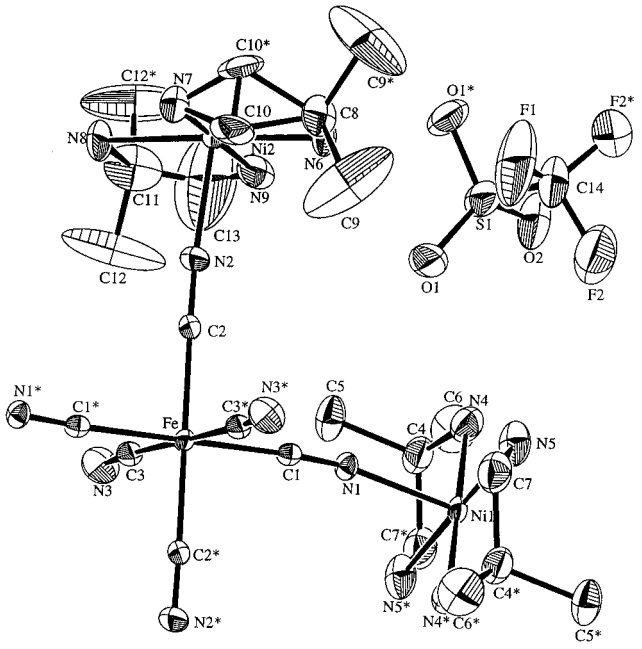

Figure 1. ORTEP view of the Ni_2Fe unit of **7** (water molecules are omitted for clarity).

Table 2. Selected bond distances (Å) and angles (deg) of **7**

	Bond Distances (Å)		
Fe−C(1)	1.99(1)	Fe−C(2)	1.92(2)
Fe−C(3)	1.97(2)	Ni(1)−N(1)	2.11(1)
Ni(1)−N(4)	2.07(2)	Ni(1)−N(5)	2.12(2)
Ni(2)−N(2)	2.11(1)	Ni(2)−N(7)	2.08(2)
Ni(2)−N(9)	2.20(2)		
	Bond Angles (deg)		
C(1)−Fe−C(2)	89.1(6)	C(1)−Fe−C(2)[a]	90.9(6)
C(1)−Fe−C(3)	88.9(5)	C(1)−Fe−C(3)[a]	91.1(5)
C(2)−Fe−C(3)	87.4(8)	C(2)−Fe−C(3)[a]	92.6(8)
N(1)−Ni(1)−N(4)	87.2(5)	N(1)−Ni(1)−N(4)[a]	92.8(5)
N(1)−Ni(1)−N(5)	95.2(5)	N(1)−Ni(1)−N(5)[a]	84.8(5)
N(4)−Ni(1)−N(5)	97.6(7)	N(4)−Ni(1)−N(5)[a]	82.4(7)
N(2)−Ni(2)−N(2)[a]	178.3(7)	N(2)−Ni(2)−N(6)	89.5(5)
N(2)−Ni(2)−N(7)	90.6(4)	N(2)−Ni(2)−N(8)	90.5(5)
N(2)−Ni(2)−N(9)	89.5(4)	N(6)−Ni(2)−N(7)	83.4(9)
N(6)−Ni(2)−N(8)	178(1)	N(6)−Ni(2)−N(9)	102(1)
N(7)−Ni(2)−N(8)	95.1(9)	N(7)−Ni(2)−N(9)	174(1)
N(8)−Ni(2)−N(9)	79(1)		
Fe−C(1)−N(1)	175(1)	C(1)−N(1)−Ni(1)	170(1)
Fe−C(2)−N(2)	178(1)	C(2)−N(2)−Ni(2)	174(1)

[a] Symmetry operation: $-x, -y, -z$.

The 2-D sheets align along the *c* axis with the intersheet Fe—Fe(0, 0, 1) separation of 10.352(7) Å (Figure 2b). The nearest intersheet Fe—Ni1 ($x + 1, y, z + 1$), Fe—Ni2 ($x, y, z + 1$), and Ni1—Ni2 ($x + 1, y + 1, z + 1$) separations are 9.91, 11.46, and 11.17 Å, respectively.

Compound 8. The asymmetric unit of 8 is given in Figure 3. The selected bond distances and angles are given in Table 3. The asymmetric unit consists of one $[Fe(CN)_6]^{3-}$ anion, one benzoate anion, two $[Ni(1,1\text{-dmen})_2]^{2+}$ cations, and six water molecules. No atom is located at a special equivalent position. The 2-D square-shaped structure is formed with the Fe−C1−N1−Ni1−N6**−C6**− and Fe−C2−N2−Ni2−N5*−C5*− linkages running along the *c* and *a* axes, respectively (Figure 4a). The intrasheet Fe—Ni1 and Fe—Ni2 separations are 5.185(3) and 5.206(6) Å, respectively. The C−N−Ni bridge angles are as follows: C1−N1−Ni1 = 168.7(6)°, C6*−N6*−Ni1 = 170.8(7)°, C2−N2−Ni2 = 170.6(6)° and C5*−N5*−Ni2 = 169.5(7)°. The Ni−N(1,1-dmen) bond lengths range from 2.103(6) to 2.137(7) Å for Ni1 and 2.092(7) to 2.138(7) Å for Ni2. The square with four Fe ions at the corners shows a slight distortion to a rhombus (interior angles: 84.3 and 95.7°). The benzoate ion resides on each square cavity with the disposition of the aromatic ring out of the cavity. Six water molecules are captured between the sheets. A disorder is seen for two water molecules whose occupancy factors are determined to be 0.5 on the basis of the peak heights.

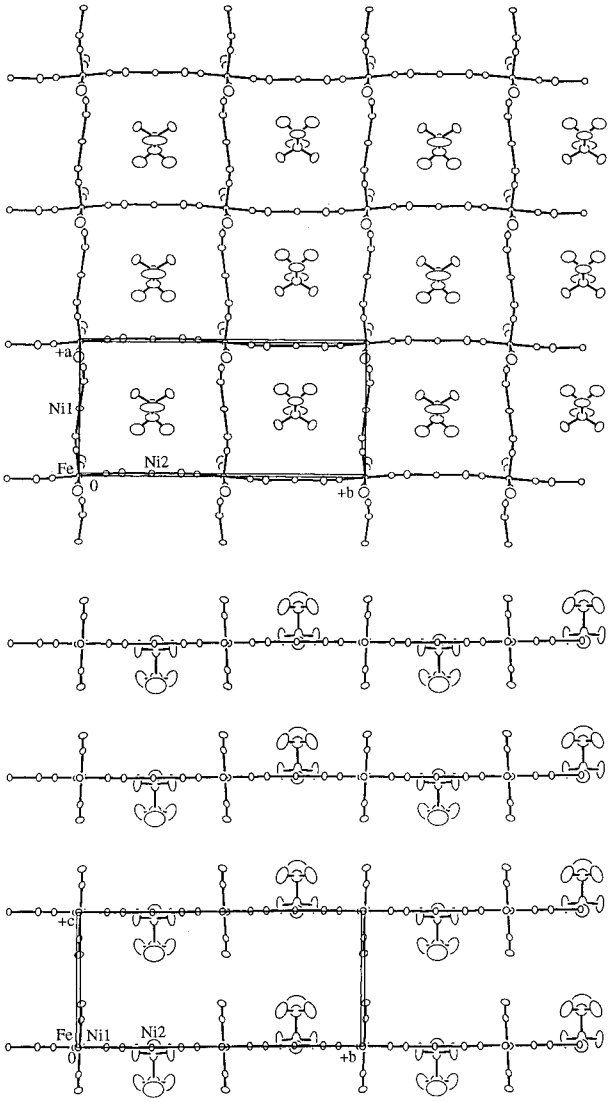

Figure 2. (**a**) A projection of the 2-D network on the *ab* plane and (**b**) the alignment of the 2-D sheets along the *c* axis for **7** (1,1-dmen and water molecules are omitted for clarity).

The packing mode of the 2-D sheets is shown by the projection onto the *ab* plane (Figure 4b). One noticeable feature is that the neighboring sheets are not in the same phase along the *b* axis. Thus, when projected on the *ac* plane, the iron of the first sheet is located above the square of the second sheet. Further, it is seen that two types of intersheet separation exist in the lattice. In one type, benzoate anions are intercalated in a head-to-head manner with respect to the benzene ring. The intersheet separation is *ca.* 11.1 Å and the nearest intersheet metal—metal separations are as follows: Fe—Fe ($-x + 1, -y$-1, $-z + 1$) = 11.863, Fe—Ni1 ($-x + 1, -y$-1, $-z + 1$) = 11.673, Fe—Ni2 ($-x + 1, -y$-1, $-z + 1$) = 11.286, Ni1—Ni1 ($-x + 1, -y$-1, $-z$) = 11.832, Ni2—Ni2 ($-x + 1, -y$-1, $-z + 1$) = 12.966, and Ni1—Ni2 ($-x + 1, -y$-1, $-z + 1$) = 11.340 Å. In another type, benzoate anion is not involved, causing a closer intersheet separation of *ca.* 10.4 Å. The nearest intersheet metal—metal separations in this type are as follows: Fe—Fe

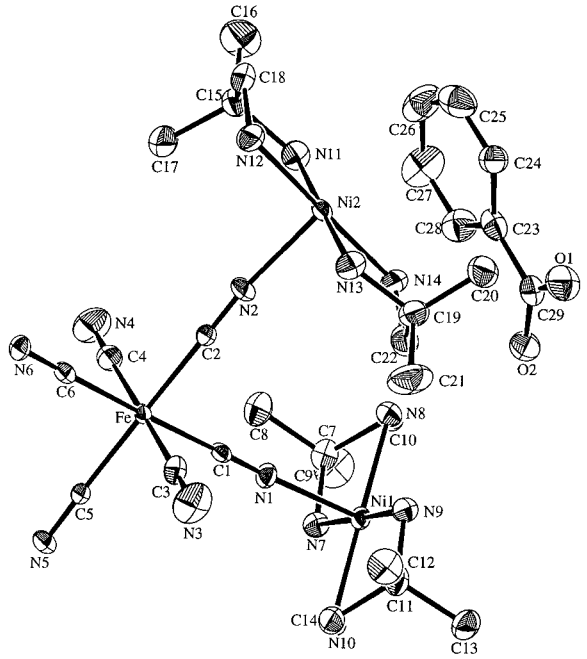

Figure 3. ORTEP view of the asymmetric unit of **8** (water molecules are omitted for clarity).

Table 3. Selected bond distances (Å) and angles (deg) of **8**

	Bond Distances (Å)		
Fe−C(1)	1.954(7)	Fe−C(2)	1.952(8)
Fe−C(3)	1.959(9)	Fe−C(4)	1.967(9)
Fe−C(5)	1.943(7)	Fe−C(6)	1.965(8)
Ni(1)−N(1)	2.110(6)	Ni(1)−N(6)	2.105(6)
Ni(1)−N(7)	2.137(7)	Ni(1)−N(8)	2.110(6)
Ni(1)−N(9)	2.114(6)	Ni(1)−N(10)	2.103(6)
Ni(2)−N(2)	2.121(7)	Ni(2)−N(5)	2.149(6)
Ni(2)−N(11)	2.098(7)	Ni(2)−N(12)	2.109(7)
Ni(2)−N(13)	2.138(7)	Ni(2)−N(14)	2.092(7)
	Bond Angles (deg)		
C(1)−Fe−C(2)	90.4(3)	C(1)−Fe−C(3)	91.5(3)
C(1)−Fe−C(4)	88.6(3)	C(1)−Fe−C(5)	90.0(3)
C(1)−Fe−C(6)	178.9(3)	C(2)−Fe−C(3)	89.4(3)
C(2)−Fe−C(4)	91.4(3)	C(2)−Fe−C(5)	178.0(4)
C(2)−Fe−C(6)	88.6(3)	C(3)−Fe−C(4)	179.2(4)
C(3)−Fe−C(5)	88.6(3)	C(3)−Fe−C(6)	89.0(3)
C(4)−Fe−C(5)	90.6(3)	C(4)−Fe−C(6)	90.9(3)
C(5)−Fe−C(6)	91.0(3)	N(1)−Ni(1)−N(6)^a	178.9(3)
N(1)−Ni(1)−N(7)	93.2(2)	N(1)−Ni(1)−N(8)	90.0(2)
N(1)−Ni(1)−N(9)	86.5(2)	N(1)−Ni(1)−N(10)	90.7(3)
N(6)^a−Ni(1)−N(7)	85.6(3)	N(6)^a−Ni(1)−N(8)	89.9(3)
N(6)^a−Ni(1)−N(9)	94.6(3)	N(6)^a−Ni(1)−N(10)	89.4(3)
N(7)−Ni(1)−N(8)	82.0(3)	N(9)−Ni(1)−N(10)	83.1(3)
N(2)−Ni(2)−N(5)^b	177.8(3)	N(2)−Ni(2)−N(11)	91.3(3)
N(2)−Ni(2)−N(12)	94.2(3)	N(2)−Ni(2)−N(13)	89.3(3)
N(2)−Ni(2)−N(14)	86.5(3)	N(5)^b−Ni(2)−N(11)	86.6(3)
N(5)^b−Ni(2)−N(12)	86.1(3)	N(5)^b−Ni(2)−N(13)	92.8(3)
N(5)^b−Ni(2)−N(14)	93.4(3)	N(11)−Ni(2)−N(12)	85.4(3)
N(13)−Ni(2)−N(14)	82.9(3)		
Fe−C(1)−N(1)	179.8(7)	C(1)−N(1)−Ni(1)	168.7(6)
Fe−C(6)−N(6)	178.8(7)	C(6)^a−N(6)^a−Ni(1)^a	169.5(7)
Fe−C(2)−N(2)	179.4(7)	C(2)−N(2)−Ni(2)	170.8(7)
Fe−C(5)−N(5)	177.9(7)	C(5)^b−N(5)^b−Ni(2)	170.6(6)

^{a} Symmetry operation: $x, y, z - 1$. ^{b} Symmetry operation: $x + 1, y, z$.

$(-x, -y, -z + 1) = 12.353$, Fe—Ni1 $(-x, -y, -z + 1) = 10.617$, Fe—Ni2 $(-x + 1, -y, -z + 1) = 12.757$, Ni1—Ni1 $(-x, -y, -z + 1) = 11.255$, Ni2—Ni2 $(-x + 1, -y, -z + 1) = 12.175$, and Ni1—Ni2 $(-x + 1, -y, -z + 1) = 10.809$ Å.

Compound 10. The asymmetric unit of **10** is shown in Figure 5, and the selected bond distances and angles are given in Table 4. The asymmetric unit consists of each one-half of

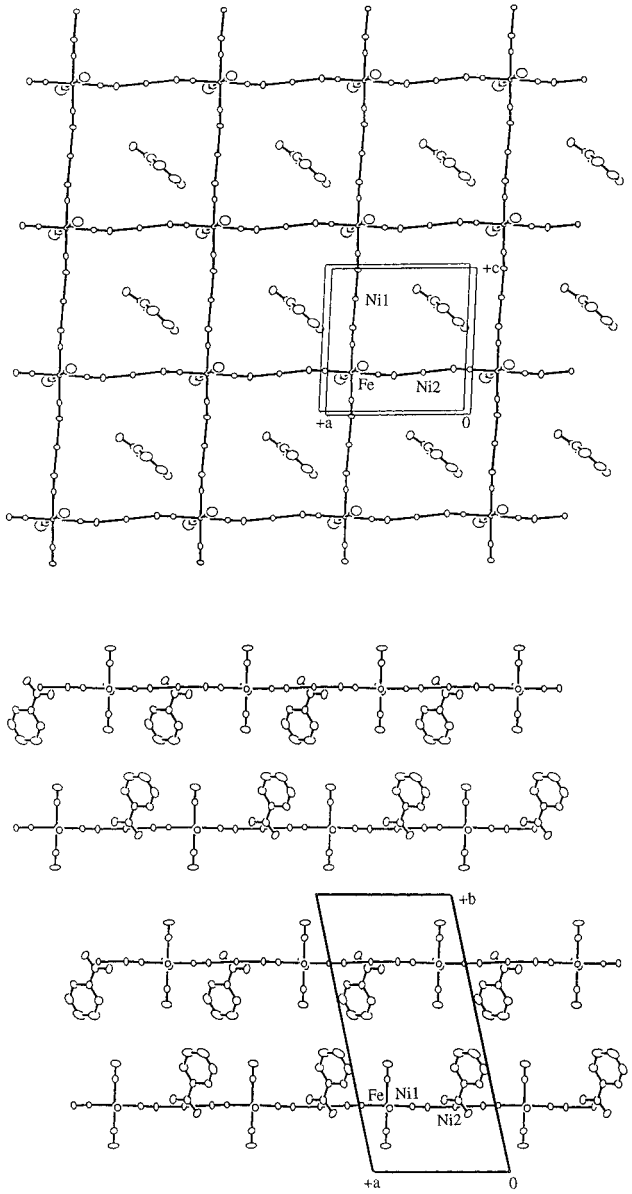

Figure 4. (**a**) A projection of the 2-D network onto the *ac* plane and (**b**) the alignment of 2-D sheets along the *b* axis for **8** (1,1-dmen and water molecules are omitted for clarity).

$[Fe(CN)_6]^{3-}$ and N_3^- anions, one-half of $[Ni(1,1\text{-dmen})_2]^{2+}$ cation, and three water molecules. All the metal ions and the N9 atom are at the special equivalent positions (Fe(0, 0, −1/2), Ni1(0, 1/2, −1/2), Ni2 (0, 0, 0), N9(0, 1/2, 0)). The projection of the polymeric structure onto the *bc* plane shows a 2-D sheet of this compound (Figure 6a). The intrasheet Fe—Ni1 and Fe—Ni2 separations are 5.173(1) and 5.112(1) Å, respectively. The square formed by four Fe ions shows a slight distortion to a rhombus (interior angles: 93.2 and 86.8°). The C1−N1−Ni1 and C2−N2−Ni2 angles are 170.3(5) and 161.6(5)°, respectively. The azide ion resides in the square cavity and aligns along one diagonal line of the square. Three water molecules are captured in the lattice, and a disorder is seen for one of the water molecules. The occupancy factors of the oxygen atoms are determined to be 0.5 on the basis of peak heights.

In Figure 6b is given the alignment of the 2-D sheets along the *a* axis. The intersheet Fe—Fe(1, 0, −1/2) separation along the *a* axis is 10.314(1) Å. The nearest intersheet Fe−Ni1 $(x + 1, y, z)$, Fe—Ni2 $(x + 1, y, z)$, and Ni1—Ni2 $(x + 1, y, z)$ separations are 11.242, 10.158, and 11.233 Å, respectively.

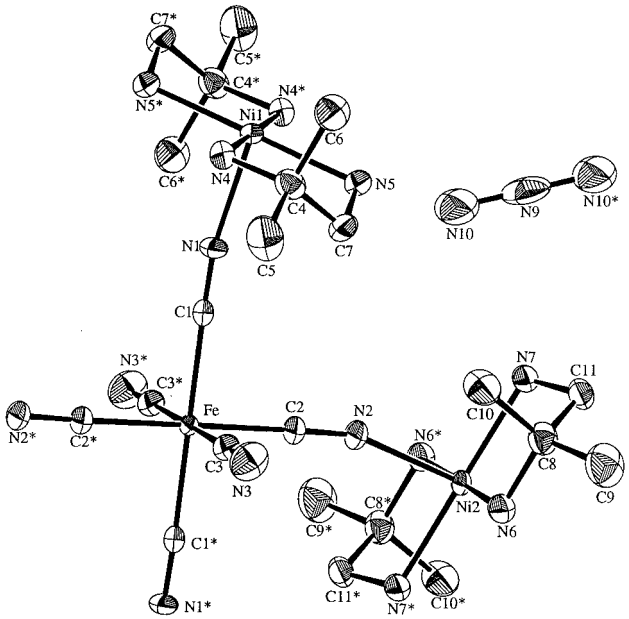

Figure 5. ORTEP view of the Ni_2Fe unit of **10** (water molecules are omitted for clarity).

Table 4. Selected bond distances (Å) and angles (deg) of **10**

	Bond Distances (Å)		
Fe−C(1)	1.955(6)	Fe−C(2)	1.942(6)
Fe−C(3)	1.937(7)	Ni(1)−N(1)	2.102(5)
Ni(1)−N(4)	2.095(5)	Ni(1)−N(5)	2.093(5)
Ni(2)−N(2)	2.105(5)	Ni(2)−N(6)	2.112(5)
Ni(2)−N(7)	2.101(5)		
	Bond Angles (deg)		
C(1)−Fe−C(2)	88.7(2)	C(1)−Fe−C(2)[a]	91.3(2)
C(1)−Fe−C(3)	90.3(2)	C(1)−Fe−C(3)[a]	89.7(2)
C(2)−Fe−C(3)	90.3(3)	C(2)−Fe−C(3)[a]	89.7(3)
N(1)−Ni(1)−N(4)	87.9(2)	N(1)−Ni(1)−N(4)[a]	92.1(2)
N(1)−Ni(1)−N(5)	87.9(2)	N(1)−Ni(1)−N(5)[a]	92.1(2)
N(4)−Ni(1)−N(5)	81.6(2)	N(4)−Ni(1)−N(5)[a]	98.4(2)
N(2)−Ni(2)−N(6)	90.3(2)	N(2)−Ni(2)−N(6)[a]	89.7(2)
N(2)−Ni(2)−N(7)	93.0(2)	N(2)−Ni(2)−N(7)[a]	87.0(2)
N(6)−Ni(2)−N(7)	81.5(2)	N(6)−Ni(2)−N(7)[a]	98.5(2)
Fe−C(1)−N(1)	178.1(5)	C(1)−N(1)−Ni(1)	170.3(5)
Fe−C(2)−N(2)	178.0(6)	C(2)−N(2)−Ni(2)	161.6(5)

[a] Symmetry operation: $-x, -y, -z$.

Some important geometrical features can be pointed out based on the above results for **7**, **8**, and **10** together with the previous result for **1**. First, in the 1,1-dmen compounds, the two methyl groups of 1,1-dmen act as a "fence" around the square cavity. Thus, the cavity has a considerable depth to accommodate various anions. In the case of the pn compounds, the cavity in the 2-D network is shallow, therefore accommodating only a limited set of counter anions. The large intersheet separation of **7**, **8**, and **10** (>10 Å) relative to that for **1** (~8.6 Å) partly relates to the steric contribution of 1,1-dmen. It is likely that the corresponding en compounds $[Ni(en)_2]_2[Fe(CN)_6]X$ (X = ClO_4^-, BF_4^-, and PF_6^-) cannot have such a 2-D network structure because the 2-D cavity formed by $[Ni(en)_2]^{2+}$ is too shallow to accommodate counter anions within it.

Secondly, the bulk structure of the bimetallic assemblies can be tuned by the counter anion X. In the case of **7** (X = $CF_3SO_3^-$) and **10** (X = N_3^-) the 2-D sheet alignment in the bulk is very similar in spite of a different space group ($P2_1/m$ for **7** and $P\bar{1}$ for **10**); both have metal ions at the special equivalent positions. In the case of **8** (X = BzO^-) of space group $P\bar{1}$, no metal ion is at a special equivalent position, and the bulk has two types of intersheet separation as discussed above. Such an anomaly in the bulk structure of **8** arises from the low-symmetric and rather bulky benzoate ion.

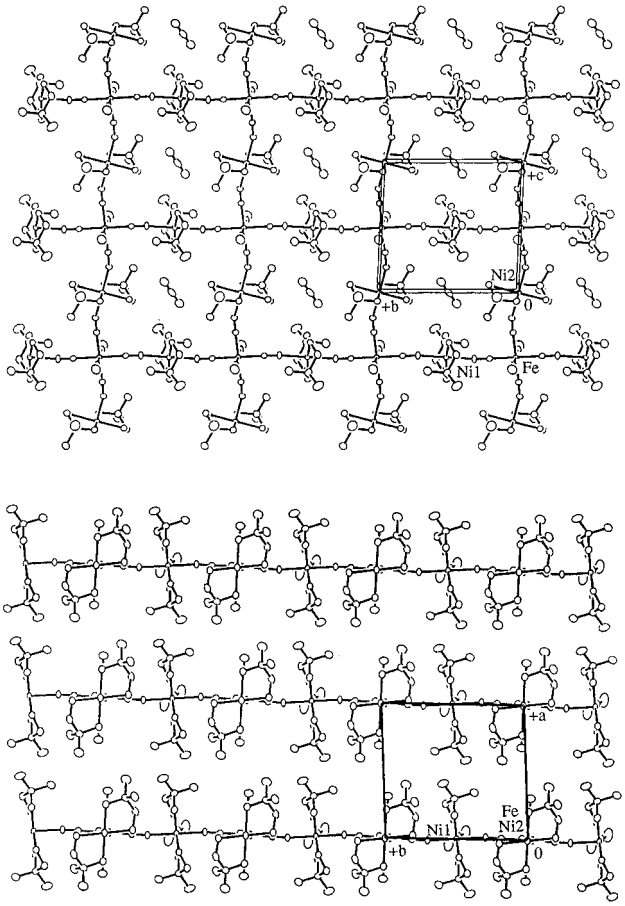

Figure 6. (**a**) A projection of the 2-D network onto the *bc* plane and (**b**) the alignment of 2-D sheets along the *a* axis for **10** (water molecules are omitted for clarity).

Finally, the hydration water plays an essential role together with the counter anion to determine the intersheet separation. For example, **7** (X = $CF_3SO_3^-$, *n* (number of hydration water) = 2) and **10** (X = N_3^-, *n* = 6) have a similar intersheet separation in spite of the different size of the counter anions. In the case of **7**, the trifluoromethyl group of $CF_3SO_3^-$ is disposed out of the square cavity (see Figure 2b) and contributes to the intersheet separation. In the case of **10**, the azide anion resides within the cavity and has little effect upon intersheet separation. Instead, six existing hydration water molecules contribute to the intersheet separation comparable to that in **7**. The significance of lattice water in bulk magnetism is discussed below.

Magnetic Properties. Pn Compounds (1−3). The magnetic behavior of **1** was preliminarily reported.[14] The $\chi_M T$ value of **1** at room temperature is 3.21 cm^3 K mol^{-1} per Ni_2Fe (5.07 μ_B) which is slightly larger than the spin-only value for one low-spin Fe^{III} and two Ni^{II} ions (2.38 cm^3 K mol^{-1}: 4.36 μ_B). Upon cooling, the $\chi_M T$ increased up to a maximum of 11.31 cm^3 K mol^{-1} (9.51 μ_B) at 10 K and then decreased below this temperature. The maximum $\chi_M T$ is larger than the value for $S_T = 5/2$ of ferromagnetically coupled Ni_2Fe (4.38 cm^3 K mol^{-1}: 5.91 μ_B), suggesting a ferromagnetic ordering of spins within the 2-D sheet. In accord with this, the $1/\chi_M$ vs. *T* plots in the temperature range 10−90 K obeyed the Curie−Weiss law with a positive Weiss constant of +7.9 K. Ferromagnetic interaction in cyanide-bridged Fe(III)($S = 1/2$)−Ni(II)($S = 1$) is known[22] and explained by the strict orthogonality of magnetic orbitals

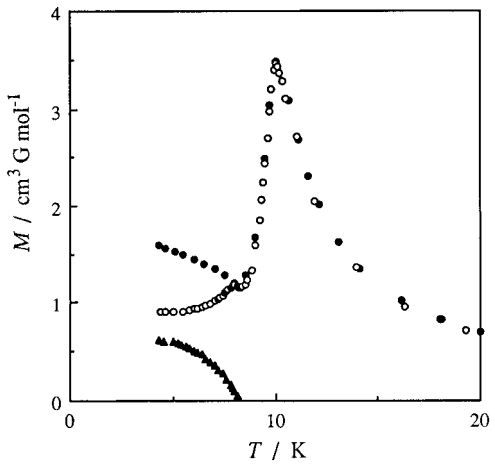

Figure 7. Temperature-dependences of magnetization for **1**: (●) field-cooled magnetization (FCM), (▲) remnant magnetization (RM), (○) zero-field-cooled magnetization (ZFCM).

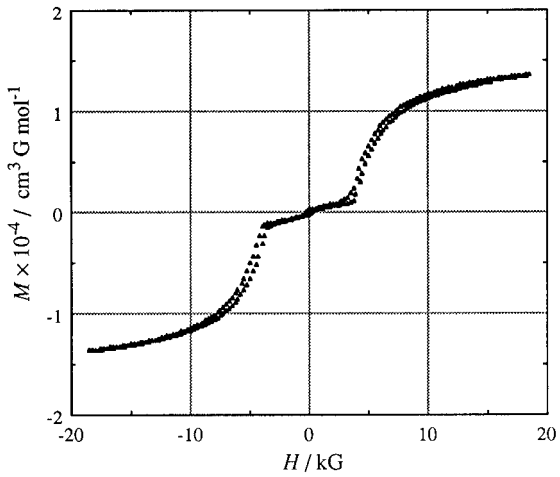

Figure 8. Magnetic hysteresis loop of **1** determined at 4.2 K.

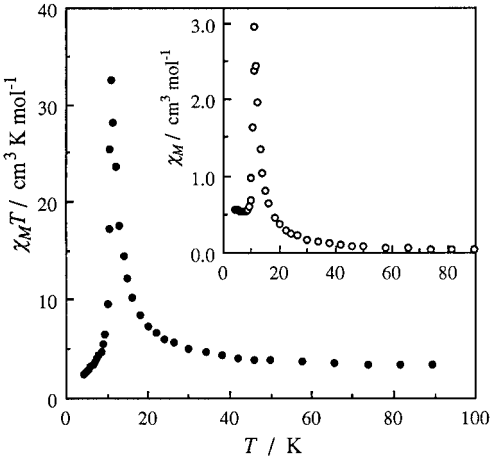

Figure 9. $\chi_M T$ vs. T plot and χ_M vs. T plot (insert) for **4**.

of the metal ions.[1] The χ_M value is 0.0105 cm^3 mol^{-1} at room temperature which increased with decreasing temperature up to a maximum value of 1.106 cm^3 mol^{-1} at 10 K, decreased down to a minimum value of 0.2987 cm^3 mol^{-1} at 6 K, and then tended to increase below 6 K. The drops in $\chi_M T$ and χ_M values below 10 K indicate the operation of an intersheet antiferromagnetic interaction. The nonzero χ_M existing in the low temperature region (< 6 K) can be attributed to a residual $\chi_\perp$ component of 3-D antiferromagnets.[23]

The increasing tendency in χ_M below 6 K suggests a magnetic ordering over the lattice. In order to confirm this, the temperature dependence of the magnetization M has been investigated in this study (see Figure 7). The field-cooled magnetization (FCM) curve obtained under a weak applied field 3 G showed a peak at 10 K and a break for saturation near 8 K. The same FCM curve was obtained under a stronger applied field 100 G. When the applied field was switched off, a remnant magnetization (RM) was observed, which decreased upon warming and vanished at 8 K. The zero-field-cooled magnetization (ZFCM) showed two maxima at 8.0 K and 9.9 K (= T_N). The peak at 8.0 K implies that the applied field is too weak to move the domain walls below this temperature. The magnetic behavior in the region of 8.0-9.9 K is typical of metamagnets.

The magnetic hysteresis loop of **1** determined at 4.2 K is given in Figure 8. The magnetization increased abruptly around 3800 G probably due to a spin flipping based on an intersheet antiferromagnetic interaction. The result adds support to the metamagnetic nature of this compound. The magnetization is not saturated at 20 kG, suggesting that each local spin is canted. The canting of the spin may arise from the magnetic anisotropy of the Ni(II) and low-spin Fe(III) ions. The RM is 400 cm^3 G mol^{-1}, and the coercive field is 290 G (see the insert). The existence of a small RM is in accord with the nonzero χ_M below 6 K.

Similar metamagnetic behavior has been demonstrated for **2** and **3**. The Weiss constant of **2** and **3** is +7.3 and +7.9 K, respectively, and the T_N is determined to be 10.1 and 9.4 K, respectively.

1,1-Dmen Compounds (4−10). The 1,1-dmen compounds are classified into two based on χ_M vs. T behavior: class A (**4**, **6**, **11**) and class B (**5**, **7**, **8**, **9**, **10**, **12**). The magnetic properties of **4** and **7** are described in detail as the representatives of the two classes.

The $\chi_M T$ vs. T plot for **4** is shown in Figure 9. The χ_M vs T plot is given in the insert. The $\chi_M T$ value at 90 K is 3.87 cm^3 K mol^{-1} per Ni_2Fe (5.56 μ_B) that is larger than the spin-only value for one low-spin Fe^{III} and two Ni^{II} ions (2.38 cm^3 K mol^{-1}: 4.36 μ_B). Upon cooling the $\chi_M T$ increased abruptly near 15 K up to a maximum value of 32.58 cm^3 K mol^{-1} (16.14 μ_B) at 11 K and then decreased below this temperature. The χ_M increased with decreasing temperature to a maximum at 11 K, decreased to a minimum at 7 K, and then increased again below 7 K. The result indicates a ferromagnetic ordering within the 2-D sheet as the dominant contribution and an antiferromagnetic interaction between the 2-D sheets as the secondary contribution (metamagnet). The $1/\chi_M$ vs. T plots in the range 11−90 K obeyed the Curie−Weiss law with a positive Weiss constant of +11.4 K.

The metamagnetic nature of **4** has been demonstrated by magnetization studies. The FCM curve measured under 3 G showed a peak at 11 K and a break for saturation near 11 K. When the applied field was switched off an RM was observed which decreased upon warming and vanished at 12 K. The ZFCM curve displayed a maximum at 11.1 K (= T_N). Similar magnetization behavior was observed for **6** and **11** (T_N = 11.0 K for **6** and 18.3 K for **11**). The magnetic hysteresis loop of **4** (determined at 4.2 K) showed an abrupt increase in magnetization around *ca.* 1800 G (see Figure 10). Thus, the spin flipping in **4** occurs under a low magnetic field (*ca.* 1800 G) relative to that of **1** (*ca.* 3800 G). This fact means that the intersheet

(22) Gadet, V.; Bujoli-Doeuff, M.; Force, L.; Verdaguer, M.; El Malkhi, K.; Deroy, A.; Besse, J, P.; Chappert, C.; Veillet, P.; Renard, J, P.; Beauvillain, P. In *Molecular Magnetic Material*; Gatteschi, D. *et al.*, Eds.; NATO ASI Series E, Kluwer, Dordrecht, 1990; Vol. 198, p 281.

(23) Carlin, R. L. *Magnetochemistry*; Springer-Verlag: Berlin, 1986.

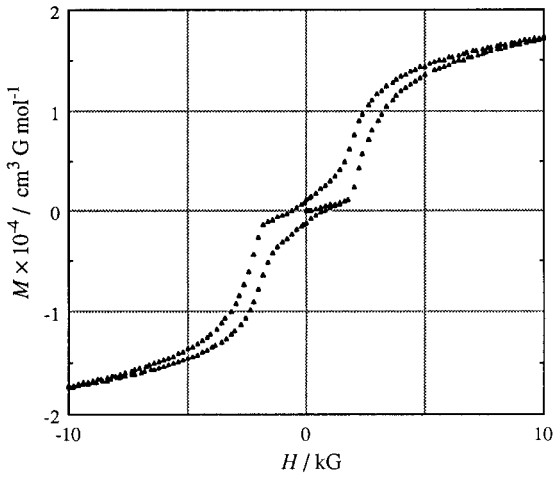

Figure 10. Magnetic hysteresis loop of **4** determined at 4.2 K.

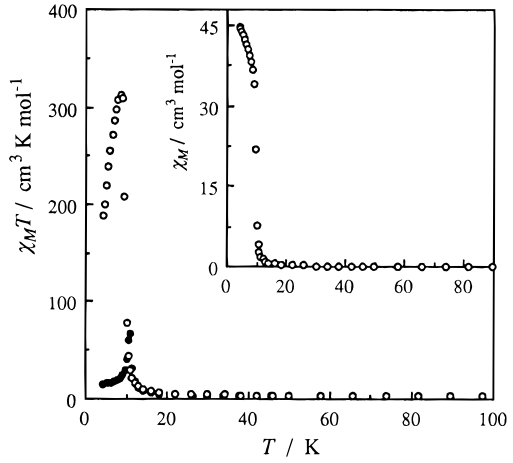

Figure 11. (a) $\chi_M T$ vs. T plots for **7** (○) and **7′** (●). The insert shows χ_M vs. T plot for **7**.

antiferromagnetic interaction in **4** is weak relative to **1**, in accord with the larger intersheet separation in the former. The RM and the coercive field are 1140 cm^3 G mol^{-1} and 600 G, respectively.

In contrast to the case of **4**, the $\chi_M T$ vs. T curve of **7** has a large maximum of 312.9 cm^3 K mol^{-1} (50.03 μ_B) at 8.5 K, and the χ_M vs. T curve showed no decrease at low temperature (see Figure 11). The Curie−Weiss plots in the temperature range of 8−50 K gave a positive Weiss constant of + 9.6 K. The sharp increase in $\chi_M T$ near 10 K up to the large maximum suggests an onset of long-range magnetic ordering. In order to prove this, the FCM, ZFCM, and RM of **7** have been measured (see Figure 12). The FCM curve displayed a sharp increase around 10 K and a tendency toward saturation at lower temperature. The ZFCM curve had a maximum of 83.84 cm^3 G mol^{-1} at 9.5 K (= T_C), and the RM observed vanished around 11 K. The other class B compounds showed similar magnetic behavior.

The magnetic hysteresis loop of **7** (4.2 K) is shown in Figure 13, and the saturation magnetization curve is given in Figure 14. In contrast to the case of **4**, the hysteresis loop shows a smooth change with the applied field. The magnetization curve shows a sharp increase from zero field. The results clearly demonstrate the ferromagnetic nature of **7**. The remnant magnetization and the coercive field are 9690 cm^3 G mol^{-1} and 250 G, respectively. It is noticeable that **8** has a large coercive field (750 G) compared with **7** (250 G) and **10** (370 G). The coercive field reflects a disorder in crystal packing, and the large

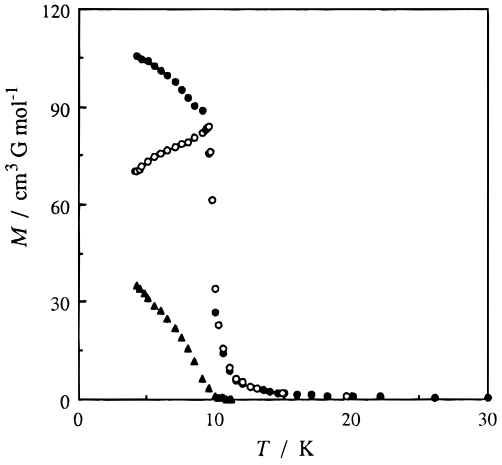

Figure 12. Temperature-dependences of magnetization for **7**: (●) field-cooled magnetization (FCM), (▲) remnant magnetization (RM), (○) zero-field-cooled magnetization (ZFCM).

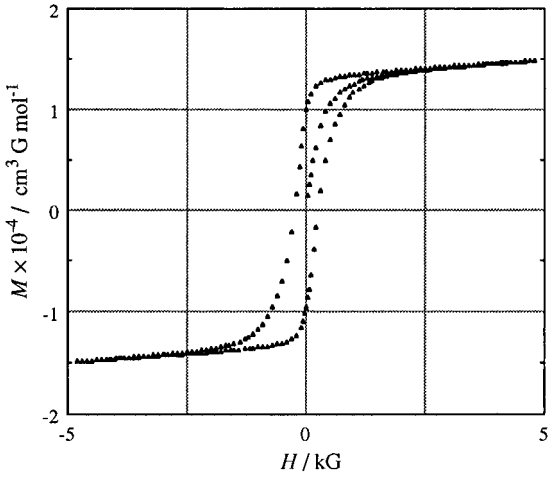

Figure 13. Magnetic hysteresis loop of **7** determined at 4.2 K.

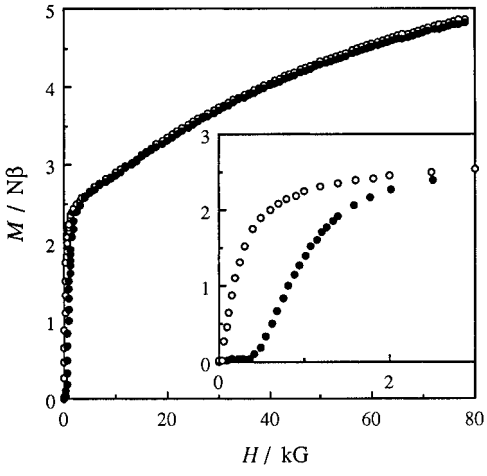

Figure 14. Saturation magnetization curves of **7** (○) and **7′** (●).

value of **8** can be ascribed to the anomaly of its bulk structure (see Figure 4b).

It is important to know what determines the ferro- or metamagnetic nature of the 1,1-dmen compounds. As discussed above, the hydration water plays an essential role in determining the intersheet separation. We may point out that class A (metamagnets) contains two hydration water molecules at best, whereas class B (ferromagnets) contains at least three lattice water molecules with one exception (**7**; $n = 2$). Despite the

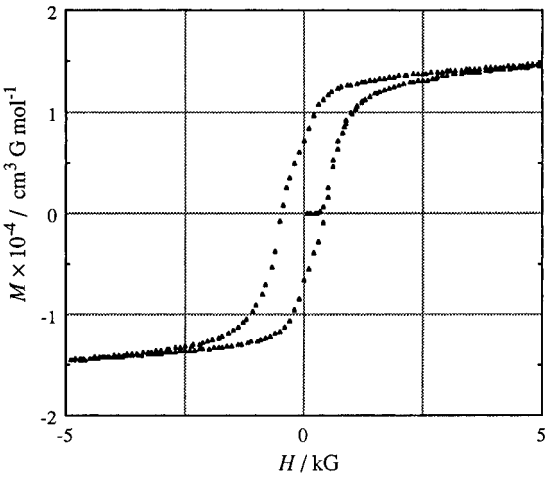

Figure 15. Magnetic hysteresis loop of **7′** determined at 4.2 K.

lack of structural information for class A, this class may have a rather small intersheet separation so as to cause a significant antiferromagnetic interaction. Class B has an intersheet separation of ca. 10 Å or larger. In this case, the intersheet magnetic interaction is negligibly weak, providing 2-D ferromagnets. One exception in class B is **7** which has only two water molecules in the lattice. In this compound, the relatively large $CF_3SO_3^-$ ion, having the trifluoromethyl group disposed out of the cavity, stands in for the lattice water as discussed before.

It is interesting to examine the dehydration effect upon the magnetic property of the class B compounds. The $\chi_M T$ vs. T curve of **7′** (the anhydrous form of **7**) is included in Figure 11. It shows a maximum value of 60.0 cm^3 K mol^{-1} (21.9 μ_B) that is much smaller than that of **7**. The Curie−Weiss plots in the range 11−90 K gave a Weiss constant +9.5 K. A long-range magnetic ordering in this compound has been proven by magnetization studies. The FCM curve showed an abrupt increase around 10 K, and the ZFCM curve has a maximum magnetization of 154.0 cm^3 G mol^{-1} at 11.1 K. The RM vanished around 12 K.

The magnetic hysteresis loop of anhydrous **7′** is shown in Figure 15. The saturation magnetization curve is given in Figure 14. Based on the hysteresis loop, **7′** appears to be a ferromagnet. However, the saturation magnetization curve shows a sigmoid feature indicating the spin flipping around 400 G. This fact clearly demonstrates the metamagnetic nature of **7′**. Evidently, the dehydration brings about a shortening in the intersheet separation and thence a significant antiferromagnetic interaction between the 2-D sheets. The spin flipping around 400 G is in line with the drop in χ_M below 11 K (see Figure 11). The RM and the coercive field of **7′** were 7200 cm^3 G mol^{-1} and 460 G, respectively. It should be noted that **7′** has a large coercive field compared with **7**. This fact indicates a disorder in the packing mode of the 2-D sheets in **7′**. The apparent ferromagnetic behavior in the magnetic hysteresis loop of **7′** may arise from a large residual ferromagnetic component based on a spin fluctuation.

Table 5. Magnetic properties of the 1,1-dmen compounds

class A (metamagnets)	n^a	T_N, K	θ, K	class B (ferromagnets)	n^a	T_C, K	θ, K
4	2	11.1	+11.4	**5**	3	14.6	+14.2
6	2	11.0	+11.1	**7**	2	9.5	+9.6
11	1	18.3	+15.7	**8**	6	9.3	+9.6
				9	4	15.2	+15.8
				10	4	9.7	+8.0
				12	4	16.2	+15.9

[a] Number of the lattice water molecules.

Similarly we have confirmed that all the class B compounds become metamagnets on dehydration. Class A compounds remain metamagnets on dehydration. The magnetic properties of the 1,1-dmen assemblies are summarized in Table 5.

Conclusions

Bimetallic assemblies [Ni(pn)$_2$]$_2$[Fe(CN)$_6$]X·2H$_2$O (X = ClO_4^- (**1**), BF_4^- (**2**), PF_6^- (**3**)) and [Ni(1,1-dmen)$_2$]$_2$[Fe(CN)$_6$]X·nH$_2$O (X = ClO_4^- (**4**), BF_4^- (**5**), PF_6^- (**6**), $CF_3SO_3^-$ (**7**), BzO^- (**8**), I^- (**9**), N_3^- (**10**), NCS^- (**11**), NO_3^- (**12**)) have a 2-D sheet of a square structure extended by Fe−CN−Ni−NC− linkages. All the assemblies show a ferromagnetic intrasheet interaction and a long-range magnetic ordering over the lattice. The magnetic nature is ferromagnetic or metamagnetic depending upon intersheet magnetic interaction. Metamagnetism appears when the intersheet separation is small enough to allow an antiferromagnetic interaction between the 2-D sheets (**1**, **2**, **3**, **4**, **6**, **11**). Ferromagnetism appears when the intersheet separation is large (>10 Å) so that the intersheet magnetic interaction is negligible (**5**, **7**, **8**, **9**, **10**, **12**). The intersheet separation is affected by the diamine ligand, the counter anion, and hydration water. Thus, the ferromagnetic compounds are available when bulky [Ni(1,1-dmen)$_2$]$^{2+}$ is used as the constituent, and three or more hydration water molecules are involved in the lattice. Dehydration of the ferromagnetic compounds causes shortening of the intersheet separation and provides metamagnets. The coercivity of the ferromagnets relates to the disorder in the packing mode of the 2-D sheets.

Acknowledgment. The authors thank Mr. Takihiro Kajio for his help in the saturation magnetization measurements.

Supporting Information Available: Tables of magnetic susceptibility and magnetization of **1**−**12** and crystallographic data, atom coordinates, anisotropic displacement parameter, thermal parameters, and bond lengths and bond angles of **7**, **8**, and **10** (92 pages). See any current masthead page for ordering and Internet access instruction.

JA962198M